Applied Catalysis B: Environmental 147 (2014) 481–489

Contents lists available at ScienceDirect

Applied Catalysis B: Environmental

journal homepage: www.elsevier.com/locate/apcatb

Glucose electrooxidation over Pd_xRh/C electrocatalysts in alkaline medium

A. Brouzgou [a], L.L. Yan [b], S.Q. Song [b,**], P. Tsiakaras [a,*]

[a] Department of Mechanical Engineering, School of Engineering, University of Thessaly, Pedion Areos, 38334 Volos, Greece
[b] State Key Laboratory of Optoelectronic Materials and Technologies/The Key Lab of Low-carbon Chemistry & Energy Conservation of Guangdong Province, School of Physics and Engineering, Sun Yat-sen University, Guangzhou 510275, China

ARTICLE INFO

Article history:
Received 19 July 2013
Received in revised form
12 September 2013
Accepted 16 September 2013
Available online xxx

Keywords:
Glucose electrooxidation
Alkaline media
Pd_xRh/C electrocatalysts

ABSTRACT

Carbon Vulcan XC-72R supported Pd_xRh (x = 1, 2, 3) nanoparticles have been prepared by a modified pulse microwave assisted polyol method and have been studied for glucose electrooxidation in alkaline media. The Pd_xRh/C electrocatalysts have been characterized by X-ray diffraction (XRD), Transmission Electron Microscopy (TEM), Cyclic Voltammetry (CV) and Chronoamperometry (CA). The effects of the concentration of electrolyte and glucose as well as of temperature on the activity of glucose electrooxidation have been investigated. According to the CV results, the electro-catalytic activity towards glucose electrooxidation of the investigated catalysts has the following order: PdRh/C > Pd/C > Pd_2Rh/C > Pd_3Rh/C. It was found that increasing electrolyte's concentration until 1.0 M KOH the current density increases, while higher (>1.0 M KOH) OH^- concentrations prevent the adsorption of glucose at the electrode. Moreover, increasing glucose's concentration from 0.02 to 0.5 M the current increases for 0.1, 0.3, 0.5, 1.0 and 2.0 M KOH. Additionally, the increment of temperature enhances glucose electrooxidation until 36.5 °C, while for temperatures >36.5 °C the catalytic activity decreases.

1. Introduction

Glucose is the most abundant carbohydrate in nature easily produced by photosynthesis in plants such as sugar cane or corn and by a large amount of waste biomass generated by agricultural activities [1,2]. The theoretical energy of glucose is 4430 W h kg^{-1} and its complete oxidation to carbon dioxide can produce 24 electrons for each glucose molecule through the following chemical reactions:

$$\text{Anode reaction}: C_6H_{12}O_6 + 24OH^- \rightarrow 6CO_2 + 18H_2O + 24e^- \quad (1)$$

$$\text{Cathode reaction}: 6O_2 + 12H_2O + 24e^- \rightarrow 24OH^- \quad (2)$$

$$\text{Overall reaction}: C_6H_{12}O_6 + 6O_2 \rightarrow 6CO_2 + 6H_2O \quad (3)$$

A potential approach to obtain energy from glucose is to be used as fuel of a fuel cell, where glucose can be directly oxidized to generate electricity, similar to direct methanol (DMFCs) [3,4] and direct ethanol fuel cells (DEFCs) [5,6].

The electrooxidation of glucose has mainly two purposes: (i) in vivo applications (as human implantable devices that will power microelectromechanical devices [7,8] and (ii) the development of glucose electrochemical sensors for diabetes check. Glucose could be virtually withdrawn without limit from the flow of blood providing a long-term or even permanent power supply for such devices as pacemakers, glucose sensors for diabetics or small valves for bladder control. Consequently, many attempts have been made mainly on the development of enzymatic and microbial glucose fuel cells. More precisely, in the past few decades most researches had been turned to the immobilization methods for enzymatic catalysts in an effort to increase the lifetime of enzymes and therefore of glucose fuel cells [9–15]. Enzymatic catalysts for glucose/O_2 fuel cells have excellent selectivity and can produce power densities of several mW cm^{-2}. However, they have very short lifetime, typically less than thirty days, due to the fragile nature of the enzymes and poor immobilization techniques. This makes them generally unsuitable for long-term implantable applications despite having been successfully tested in-vivo. Thus, recently, there has been an increasing interest in non-enzymatic glucose fuel cells where platinum [16–21] and gold alloys [16,20–23] are mainly used as anode electrocatalysts and usually activated carbon as cathode electrocatalyst [24–26]. The reported results prove that such fuel cells present much better stability having been successfully tested in-vivo [27]. However, the poor anode selectivity towards glucose oxidation in the presence of oxygen is still the biggest challenge for direct in-vivo glucose fuel cells. Recently, Kerzenmacher *et al.* [7,8,28] proposed novel direct glucose fuel cell (DEFC) structures

* Corresponding author. Tel.: +30 24210 74065; fax: +30 24210 74050.
** Corresponding author. Tel.: +86 20 84113253; fax: +86 20 84113253.
E-mail addresses: stsssq@mail.sysu.edu.cn (S.Q. Song), tsiak@uth.gr (P. Tsiakaras).

0926-3373/$ – see front matter © 2013 Elsevier B.V. All rights reserved.
http://dx.doi.org/10.1016/j.apcatb.2013.09.024

with Raney platinum or Raney platinum doped with zinc electrodes as anode and thin layer platinum as cathode, and they examined their compatibility with a body tissue environment. The Raney-platinum fuel cells exhibited a power density of up to (4.4 ± 0.2) $\mu W\,cm^{-2}$ with 7.0% oxygen saturation, despite the limited oxygen supply. This high performance was attributed to the increased oxygen tolerance of the Raney-platinum film anodes.

At present, Pt [17,29,30], Au [22,31] and their bi-metallic catalysts, Pt-Bi [25], Pt-Pd [32], Pt-Ru [24], Pt-Au [21,26], Ag-Au [33–35] and their tri-metallic catalysts [36] have been studied for glucose electrooxidation. There are also some researches [37–40] that have examined Pd-based electrocatalysts for glucose electrooxidation. It has been proved [41] that Pd presents better activity than Pt and Au towards alcohols electrooxidation in alkaline media, reducing at the same time the high cost of the electrodes, if it is considered that last year the cost of platinum was doubles that of palladium [42]. However, the cost of rhodium was almost the same as platinum's one [42]. For this reason, electrocatalysts with very low rhodium amount are also studied and investigated in the present manuscript.

Here, we report for first time the study of glucose electrooxidation at 20 wt.% Pd_xRh/C ($x = 1$, 2, 3) electrocatalysts. Since in literature there is no similar work, this constitutes a novelty and a first step for further investigation of modified PdRh/C electrocatalysts. The home-made electrocatalysts were physicochemically characterized by X-ray diffraction (XRD) and transmission electron microscope (TEM) techniques. Cyclic voltammetry (CV) and Chronoamperometry (CA) techniques were used to evaluate their electrocatalytic activity and their stability to glucose electrooxidation. The results are compared with those of a home-made carbon supported Pd (Pd/C) (20 wt.% metal).

2. Experimental

2.1. Materials

Carbon powder Vulcan XC-72R (Cabot Corporation) was used as support. $PdCl_2$ and $RhCl_3$ were used as the corresponding metal precursors. All aqueous solutions were prepared by ultrapure water (18.2 MΩ cm Millipore–Milli-Q) during catalysts preparation. Ethanol (>99% purity) (Sigma Aldrich) and Nafion® (5 wt.%, IonPower, GmbH) were used for catalyst ink preparation. D-glucose (99.5% pure, assay) and KOH (>85% assay, flakes purified) were provided by Sigma Aldrich.

2.2. Catalysts preparation

The 20 wt.% Pd_xRh/C ($x = 1$, 2, 3 denotes the Pd:Rh molar ratio) electrocatalysts were fast and easily prepared by the pulse-microwave assisted polyol synthesis method [43]. The primary steps of this synthesis process are given as follows: The starting precursors ($PdCl_2 \bullet 2H_2O$ and $RhCl_3$) were well mixed in a beaker with ethylene glycol (EG) by the aid of an ultrasonic bath, and then XC-72R carbon black was added into the mixture. After the pH value of the system was adjusted to be ~13 by the dropwise addition of 1.0 mol L^{-1} NaOH/EG, a well-dispersed slurry was obtained by ultrasonic stirring for 30 min. Thereafter, the slurry was microwave-heated for several times in a 10 s-on/10 s-off pulse form. In order to promote the adsorption of the suspended metal nanoparticles onto the support, hydrochloric acid was adopted as the sedimentation promoter and the solution was re-acidified to a pH value of about 3–4. The resulting black solid sample was filtered, washed with hot de-ionized water and dried at 80 °C for 10 h in a vacuum oven. For the sake of comparison, 20 wt.% Pd/C was also prepared in the same way and examined under the same experimental conditions for the glucose electrooxidation.

2.3. Physicochemical characterization

The X-ray Diffraction (XRD) measurements were carried out by the aid of a D/Max-IIIA (Rigaku Co., Japan) employing Cu K_α ($\lambda = 0.15406$ nm) as the radiation source. The samples were scanned in the range of $10° \leq 2\theta \leq 86°$. The peak at 68° (Pd 2 2 0) was used for the calculation of crystallite size. Catalysts were also investigated by transmission electron microscopy (TEM) using a Philips CM12 microscope (resolution 0.2 nm), provided with high resolution camera, at an accelerating voltage of 120 kV.

Suitable specimens for TEM analyses were prepared by ultrasonic dispersion in *i*-propylic alcohol adding a drop of the resultant suspension onto a holey carbon supported copper grid. To prevent the agglomeration of carbon supports, the prepared catalyst was diluted in ethanol using ultrasonic water bath for some minutes and dried before TEM analysis. High dilution helps to separate the catalyst particles from each other.

2.4. Electrochemical characterization

Three-electrode cell assembly connected to electrochemical station (AMEL 5000) was used for the CV and CA measurements. Hg/HgO (in 1.0 mol L^{-1} KOH) and ($d = 12$ mm, $A = 1.1$ cm^2) were adopted as reference and counter electrodes, respectively. The working electrode was a glassy carbon electrode ($d = 3.0$ mm, $A = 0.07$ cm^2). The catalyst slurry was prepared with the aid of magnetic stirrer, dispersing 5.0 mg of the as-prepared electrocatalyst powder in 1.8 mL ethanol and 0.2 mL Nafion® ionomer for 40 min [44]. The catalyst ink was then quantitatively (10 μL) transferred onto the surface of the glassy carbon disk electrode by using a micropipette and dried under infrared lamp to obtain a catalyst thin film. Initially, in order to find out the most active electrocatalyst towards glucose electrooxidation, CV measurements were carried out in aqueous solution containing 0.5 mol L^{-1} KOH in absence and in presence of 0.5 mol L^{-1} glucose. Before each measurement the solution was deareated for 30 min with high-purity nitrogen gas to remove the dissolved oxygen from the aqueous solution. The potential window ranged from −0.8 to 1.2 V (vs. Hg/HgO) at a sweeping rate of 20 mV s^{-1}. Additionally, the effects of glucose's (0.02, 0.05, 0.2 and 0.5 mol L^{-1}) and the electrolyte's concentration (0.1, 0.3, 0.5, 1.0 and 2.0 mol L^{-1} KOH) were separately investigated over the PdRh/C electrocatalyst which presented the best performance among the examined electrocatalysts. Moreover, the influence of temperature and scan rate in 0.5 mol L^{-1} KOH containing 0.5 mol L^{-1} glucose aqueous solution was studied. It should be noted that the potential is referred to Hg/HgO (1 mol L^{-1} KOH) reference electrode without specification.

3. Results and discussion

3.1. Physico-chemical characterization of Pd_xRh/C

XRD patterns of the as-prepared electrocatalysts are shown in Fig. 1. As it is observed there are no noticeable peaks for phase-separated structures such as Rh metals, which is probably due to the formation of Pd_xRh/C alloys, reported also in literature [45]. The first peak at 25° is associated with the Vulcan XC-72 support material for all the four samples. There are five observed characteristic diffraction peaks at *ca.* 38°, 45°, 65°, 79° and 83° belonging to the face-centred cubic (fcc) phase of Pd (1 1 1), (2 0 0), (2 2 0), (3 1 1) and (2 2 2), respectively. The Pd (1 1 1) plane has the largest intensity among those planes, which becomes more intense as the

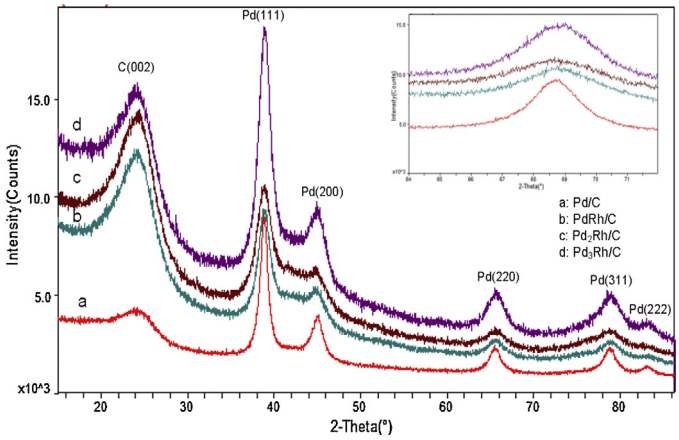

Fig. 1. XRD results of the as-prepared carbon supported Pd_xRh/C electrocatalysts.

Table 1
Structural parameters of the as-prepared catalysts.

Catalysts	Crystallite size (nm)	Lattice parameter (nm)	Particle size (nm)
Pd/C	8.2	0.3865	$8.0 < d < 10.0$
PdRh/C	7.0	0.3859	$5.0 < d < 10.0$
Pd_2Rh/C	22.0	0.3880	$5.0 < d < 12.0$
Pd_3Rh/C	14.0	0.3896	$5.0 < d < 10.0$

palladium ratio increases (Pd_3Rh/C) [46]. Moreover as the palladium ratio increases the Pd (1 1 1) peak position slightly shifts to more positive angles (Pd/Rh/C: 38.826°, Pd_2Rh/C: 38.96°, Pd_3Rh/C: 38.81°) indicating that part of the Rh has been alloyed with Pd [47].

In Table 1, the crystallite size and the corresponding lattice parameters calculated from the Pd (2 2 0) diffraction (Fig. 1 inset) line using the Scherrer formula and Bragg equations are summarized [48,49]. It can be clearly seen that the lattice parameter decreases in the following order: $Pd_3Rh/C > Pd_2Rh/C > Pd/C > PdRh/C$.

The surface morphology of the prepared Pd_xRh/C electrocatalysts was examined by TEM. TEM images in Fig. 2 (A–D) show a successful loading dispersion of PdRh/C and Pd_3Rh/C, Pd/C nanoparticles onto the surface of carbon substrate.

However, many agglomerates and a relatively poor dispersion are observed for the Pd_2Rh/C electrocatalyst. However, it is believed that this factor cannot be the main reason for its lower electrocatalytic activity as discussed below, according to the electrochemical evaluation, since Pd_3Rh/C which presents the lowest activity does not form so many agglomerates.

3.2. Electrochemical characterization

3.2.1. Glucose electrooxidation

In Fig. 3 (A and B) the voltammetric curves of Pd/C, PdRh/C, Pd_2Rh/C and Pd_3Rh/C electrocatalysts in 0.5 mol L^{-1} KOH (Fig. 3 (A)) and in 0.5 mol L^{-1} KOH + 0.5 mol L^{-1} glucose (Fig. 3 (B)) are depicted. In the case of Pd-based electrocatalysts the electrochemical active surface area (S_{ESA}) is calculated by determining the coulombic charge (Q) for the reduction of palladium oxide (peak IV in Fig. 3 (A)) [50]. The S_{ESA} values, reported in Table 2, are estimated using the following equation:

$$S_{ESA}\ [m^2_{pd/g_{pd}}] = \frac{\text{charge}\ [\mu C\ cm^{-2}]}{\{405\ [\mu C\ cm^{-2}_{pd}] \times Pd_{loading}\ [mg\ cm^{-2}]\}} \times 10 \quad (4)$$

A charge value of 405 μC cm^{-2} is assumed for the reduction of PdO monolayer [51]. The calculated electrochemical active surface areas have the following order of PdRh/C > Pd_2Rh/C > Pd_3Rh/C > Pd/C.

In Fig. 3 (A) during the positive-going sweep, three oxidation peaks can be observed, which correspond to different electrochemical processes occurring at the surface of the Pd electrode [52]. Peak I in the potential range between −0.6 and −0.4 V is due to the oxidation of the absorbed hydrogen [53–55]. Peak III, which emerges above −0.25 V, could be attributed to the formation of palladium (II) oxide layer at the surface of the catalyst. Although the mechanism of this oxidation process remains unclear, it has been widely accepted that OH^- ions are firstly chemisorbed in the initial stage of the oxide formation, and then at higher potentials they are transformed into higher valence oxides, as described in the literatures [55–57]. The adsorption of OH^- starts at the far negative potential from the onset potential of the Pd oxidation (peak II). As it can be observed peak II is more intense for the Pd/C sample. Finally, peak IV can be attributed to the reduction of the Pd(II) oxide during the cathodic sweep [55,56].

Fig. 3 (B) shows the cyclic voltammograms of the Pd_xRh/C and Pd/C electrocatalysts in 0.5 mol L^{-1} solution containing 0.5 mol L^{-1} glucose. As it can be seen, the electrocatalytic activity towards glucose electrooxidation has the following order: PdRh/C > Pd/C > Pd_2Rh/C > Pd_3Rh/C. In the case of lower Rh content, its effect on Pd's activity towards glucose electrooxidation is decreased. Moreover the onset potential for PdRh/C is much lower than that of the other electrocatalysts. As far as Pd/C electrocatalyst is concerned, despite the fact that it presents high activity, the onset potential of glucose oxidation shifts to higher potential (more positive) values and the peak potential also occurs at higher potential value.

During the forward scan one peak is formed for all the examined electrocatalysts, which can be attributed to the formation of palladium oxides [58] and glucose electrosorption of glucose to form an adsorbed intermediate. The decrease in current at potentials more positive with respect to the peak potential could be due to the formation of thick palladium oxide which competes for surface adsorption sites with glucose and in turn inhibits the electrooxidation of glucose as well [59]. During the reverse scan, oxidation of glucose happens, in the potential region in which the surface oxides are reduced. The reduction of the surface palladium oxides occur at potential values more negative than −0.1 V and enough surface active sites are available for the direct oxidation of glucose. Therefore, there is a sharp increase in anodic current with the peak at −0.10 V for the Pd/C and at −0.16 V for the rest electrocatalysts. By shifting the potential to more negative values, the electrosorption of glucose on the catalyst surface starts again, resulting in the

Table 2
Electrocatalytic kinetic parameters at different electrodes in 0.5 mol L^{-1} KOH, at room temperature, 20 mV s^{-1}.

Catalysts (20 wt%)	Pd loading (μg cm^{-2})	EASA ($m^2\ g^{-1}$)	Onset potential (V *vs.* Hg/HgO)	Peak potential (V *vs.* Hg/HgO)	I_f (peak current density, mA cm^{-2})	I_b (peak current density, mA cm^{-2})
Pd/C	72.0	10.3	−0.19	0.11	2.7	1.6
PdRh/C	36.0	26.0	−0.55	0.051	3.5	0.9
Pd_2Rh/C	48.2	14.8	−0.34	0.048	1.9	0.6
Pd_3Rh/C	54.0	12.8	−0.34	0.043	1.7	0.2

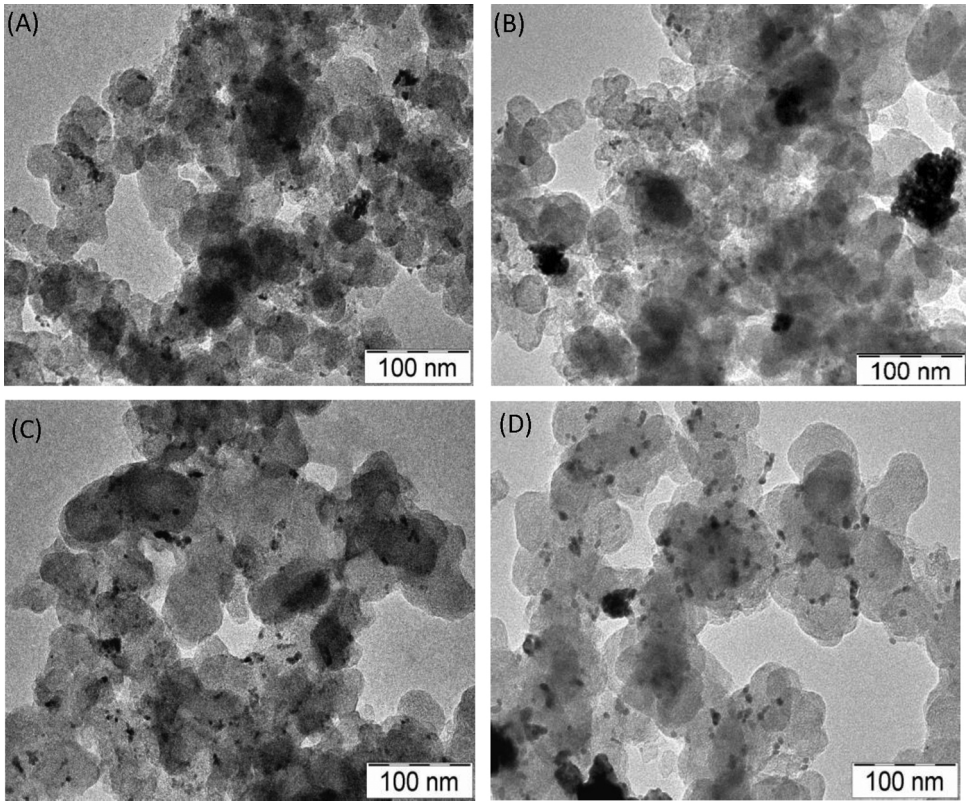

Fig. 2. TEM images of (A) PdRh/C, (B) Pd_2Rh/C, (C) Pd_3Rh/C and (D) Pd/C.

accumulation of intermediates at the electrocatalyst surface leading again to the decrease of the anodic current as it is shown in Fig. 3 (B).

3.2.2. Effect of concentration of electrolyte and glucose

The effect of different: (i) KOH concentrations of 0.1, 0.3, 0.5, 1 and 2.0 mol L^{-1} and (ii) glucose concentrations of 0.02, 0.05, 0.2 and 0.5 mol L^{-1}, for the reaction of glucose electrooxidation, are investigated at PdRh/C electrocatalyst, which present the highest catalytic activity to glucose electrooxidation (Fig. 3 (B)). The results are presented in Fig. 4.

The oxidation current increases almost linearly as the KOH concentration increases from 0.1 to 1.0 mol L^{-1}. However, further increase in the concentration of KOH (>1 M KOH) leads to a decrease of the peak current density. The same behaviour was observed by Liang *et al.* [52]. From this behaviour one might deduce that glucose oxidation can be accelerated by the presence of OH^- anions, leading to an increase in the anodic peak. However, at concentrations higher than 1.0 M KOH the adsorption of the OH^- anions at Pd prevents the adsorption of glucose at it [52]. Furthermore, the peak potential shifts to more negative values with the increase of KOH's concentration, while at all the examined electrolyte's concentration values, the peak potential shifts to more positive values with the increase of glucose's concentration. The maximum current density reaches 5.2 mA cm^{-2} for 1.0 mol L^{-1} KOH containing 0.5 mol L^{-1} glucose. In Fig. 4 (F), the

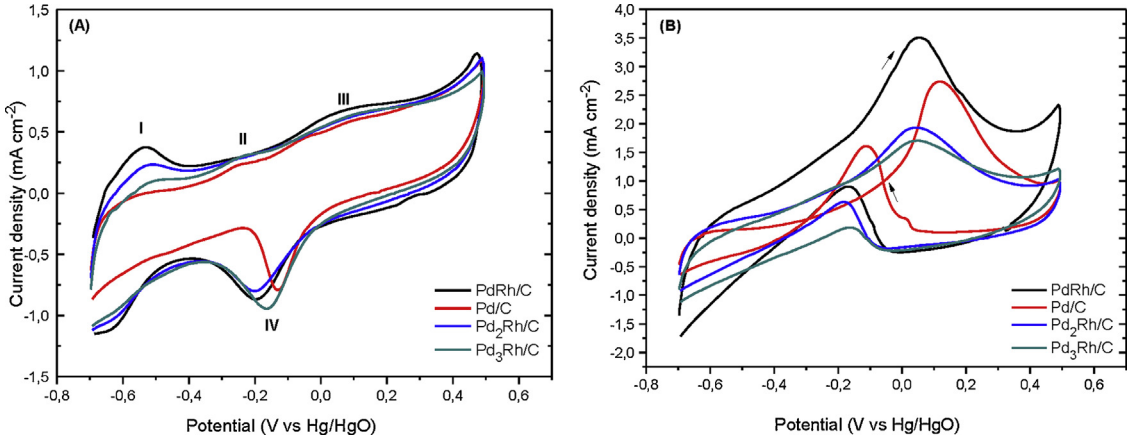

Fig. 3. Cyclic voltammograms of the Pd_xRh/C electrocatalysts in: (A) 0.5 mol L^{-1} KOH solution and (B) 0.5 mol L^{-1} KOH containing 0.5 mol L^{-1} glucose (scan rate: 20 mV s^{-1}, room temperature).

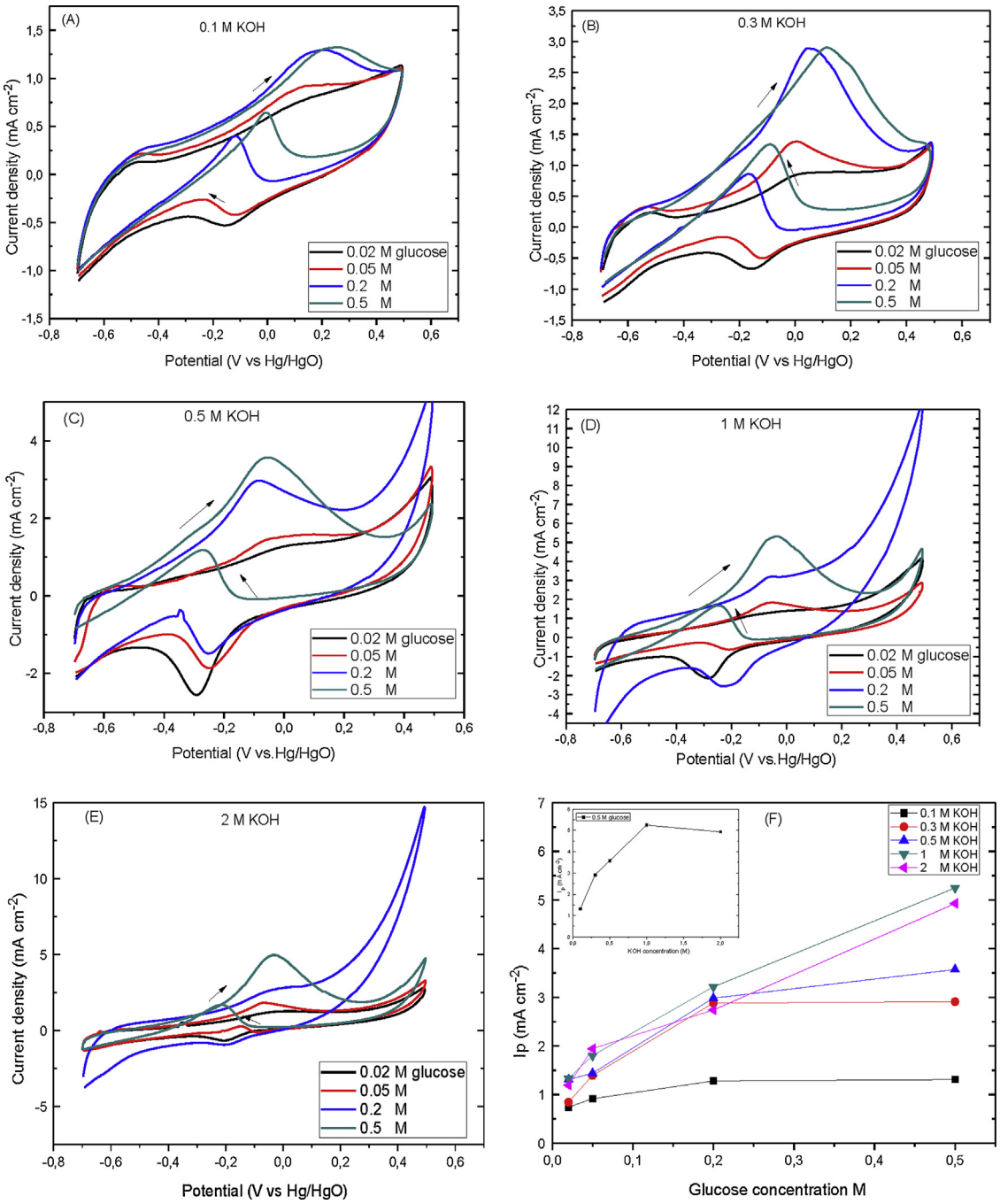

Fig. 4. Cyclic voltammograms of the PdRh/C electrocatalyst in: (A) 0.1, (B) 0.3, (C) 0.5 (D) 1 and (E) 2 mol L^{-1} KOH containing *y* (=0.02, 0.05, 0.2, and 0.5 mol L^{-1}) glucose (scan rate: 20 mV s^{-1}, room temperature). Fig. 4 (F): Peak current density dependence on glucose concentration for 0.1, 0.3, 0.5, 1.0 and 2.0 M KOH.

dependence of peak current density on glucose concentration is plotted.

Tafel plots are obtained from the onset region of the polarization curves [60] from the limiting form of the Butler–Volmer:

$$\log \quad i = \log \quad i_o + \left(\frac{\alpha_a nF}{2.303RT}\right)\eta \tag{5}$$

where η is the overpotential, i_o is the exchange current density and α_a is the anodic transfer coefficient, n is the electron number involved in the reaction, F is the Faraday's constant, R is the universal gas constant and T the temperature.

In Fig. 5 (A) the voltammetric curves for glucose electrooxidation taken for 5 mV s^{-1} scan rate are depicted. In order to reduce the mass transfer effect as much as possible and to derive kinetic parameters the scan rate was low. Fig. 5 (B) derives from Fig. 5 (A) and the exchange current density is calculated according to Ref. [60]. From Fig. 5 (B) the exchange current density values (i_o) are calculated: 0.02, 0.09, 0.12 and 0.17 mA cm^{-2}, for 0.02, 0.05, 0.2 and 0.5 mol L^{-1} glucose, respectively. The calculated values of the exchange current densities according to literature [61] are reasonable. However, due to lack of literature concerning electrokinetic data for glucose the results cannot be compared with the others. From the low values of the exchange current density it is

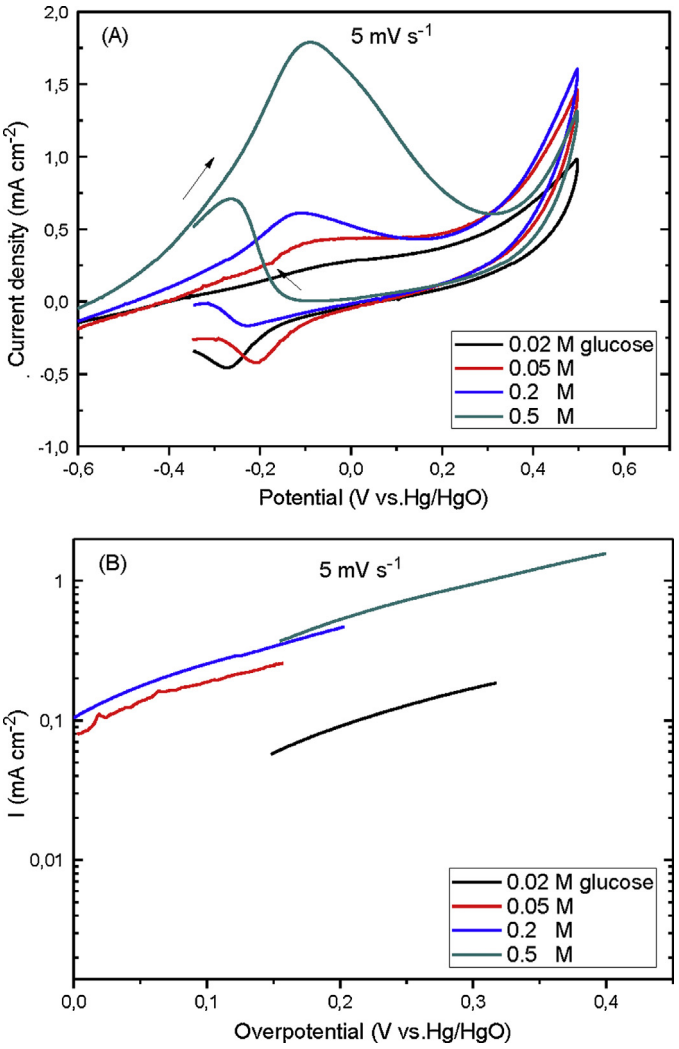

Fig. 5. (A) Cyclic voltammograms of PdRh/C electrocatalyst in 0.5 mol L^{-1} KOH containing (=0.02, 0.05, 0.2, and 0.5 mol L^{-1}) glucose (scan rate: 5 mV s^{-1}, room temperature), (B) Tafel plots derived from Fig. 5 (A).

obvious that further research is necessary in order to obtain higher activity.

3.2.3. Effect of varying potential sweep rate

The effect of scan rate on the peak current density at PdRh/C in 0.5 mol L^{-1} KOH + 0.5 mol L^{-1} glucose is shown in Fig. 6 (A). It is observed that the peak current density increases rapidly by increasing the potential scan rate from 5 to 200 mV s^{-1}. Moreover, the shift of the peak potential to higher values is possibly due to the IR drop generated at high current density values [62].

The linear relationship between the square root of the scan rate and the peak current density (Fig. 6 (B)), proves that the control of the overall glucose oxidation reaction is controlled by the mass transport of the glucose from the bulk solution to the electrode surface [63]. As it is observed the line does not cross through the origin which can be ascribed to the fact that the rate-determining step of glucose oxidation involves adsorption and diffusion. Similar results have been also reported from Hu et al. [64].

In general, for an electrochemical oxidation reaction, the linear relationship between E_p and ln(ν) can be represented by the following equation [65–67]:

$$E_p = A + \left(\frac{RT}{(1-a)nF}\right) \ln \quad \nu \tag{6}$$

From Fig. 6 (C) it can also be seen that the E_p (positive scan) rises with the increase of ν and shows the linear relationship between E_p and ln(ν), indicating that the oxidation of glucose is an irreversible charge transfer process. The irreversibility of the reaction is also obvious from the cyclic voltammogram curves, since the reduction curve continues at positive current density values. In case of reversibility the reduction curve should be the mirror (negative current densities) of the first oxidation peak.

From the slope of $E_p - \ln \nu$ the transfer coefficient was calculated (giving $n = 2$). In fact, two electrons are involved, since glucose electrooxidation at present investigated conditions follows the following process:

$$C_6H_{12}O_6 + 2OH^- \rightarrow C_6H_{12}O_7 + H_2O + 2e^- \tag{7}$$

The α value was calculated 0.69 > 0.5, indicating according to the theory of analytical electrochemistry [68,69] an irreversible diffusion control process. Comparing the result with other works in literature the calculated value is reasonable. Becerik [70] studied glucose electrooxidation at platinum-palladium electrodes calculating $\alpha = 0.4$, while Hu *et al.* [64] studying the electrooxidation of glucose at palladium predicted $\alpha = 0.5$. According to the above-results the glucose oxidation process has been described also as nearly-irreversible.

3.3. Effect of temperature

The effect of temperature (T = 25–60 °C) on the electrooxidation of glucose is also investigated. Fig. 7 (A) shows the CVs at the PdRh/C electrode for glucose oxidation at different temperature values. The increase in temperature causes an evident increase in the anodic peak current density until 36.5 °C. This behaviour is justified since it agrees with the results reported by Yei *et al.* [71]. According to them glucose degraded rapidly above 40 °C as evidenced by a rapid change of colour to yellow-brown and caramel like smell. The same degradation phenomena were also observed during our experiments. As it is observed, in Fig. 7 (A), increasing the temperature the baseline of the cyclic voltammograms curves shifts up to higher current densities. However, the net current density decreases for T > 36.5 °C. The same behaviour was observed for the rest electrocatalysts.

The activation energy E_a can be obtained from the currents measured at different temperatures using the following equation:

$$E_a = R\left(\frac{d(\ln \quad I)}{d(1/T)}\right) \tag{8}$$

The activation energy E_a was calculated at specific potential value (at 0.06, 0.24, 0.24 and 0.097 V, for PdRh/C, Pd_2Rh/C Pd_3Rh/C and Pd/C, respectively) from the cyclic voltammograms in 0.5 mol L^{-1} KOH containing 0.5 mol L^{-1} glucose at 5 mV s^{-1} [72]. The activation energy E_a was calculated to be 25.0, 24.3, 31.0 and 43.0 kJ mol^{-1} for the PdRh/C, Pd/C, Pd_2Rh/C and Pd_3Rh/C, respectively. Low activation energy means high intrinsic activity and consequently faster charge-transfer process [73]. Obviously, PdRh/C electrocatalyst exhibits the highest activity to glucose electrooxidation among the investigated samples. The estimated activation energy values almost coincide with those estimated by Hu *et al.* [64], implying that the formed $PdOH_{ads}$ exhibits a catalytic property for glucose electrooxidation similar to a radical reaction.

3.3.1. Chronoamperometric measurements

Chronoamperometric experiments were carried out to observe the stability and possible poisoning of the catalysts under short time continuous operation. Fig. 8 depicts the evaluation of activity

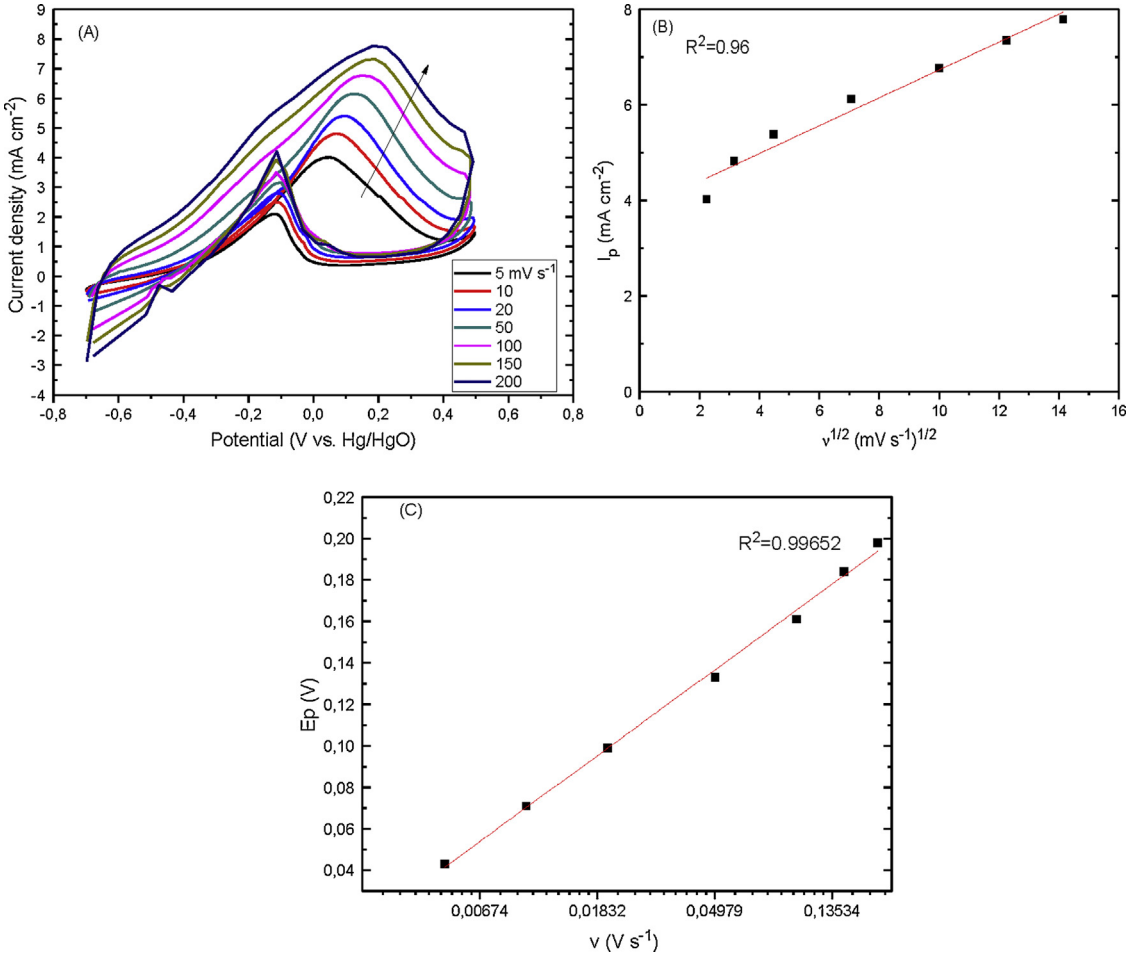

Fig. 6. (A) Cyclic voltammograms of the PdRh/C electrocatalyst in 0.5 mol L^{-1} KOH containing 0.5 mol L^{-1} glucose at different scan rates at room temperature, (B) Anodic peak current density vs. square root of scan rate, extracted from Fig. 6 (A), (C) Peak potential vs. ln(v) extracted from Fig. 6 (A).

of PdRh/C, Pd_2Rh/C, Pd_3Rh/C and Pd/C electrodes along with time at a constant applied potential of −0.13 V for 1300 s.

The long-term poisoning rate (d) is calculated by measuring the linear decay of the current for a period of more than 500 s from Fig. 7 by using the following equation [74].

$$\delta = (100/Io)(dI/dt), \quad t > 500\,\text{s} \tag{9}$$

where (dI/dt), $t > 500$ s, is the slope of the linear portion of current decay and I_o is the current at the start of polarization back extrapolated from the linear current decay. The poisoning rate is found to be 0.01, 0.0056, 0.018 and 0.0019% s^{-1} for the PdRh/C, Pd_2Rh/C, Pd_3Rh/C and Pd/C, respectively. From the values, obviously, the poison rate at PdRh/C is the highest one, which means that it is more easily poisoned.

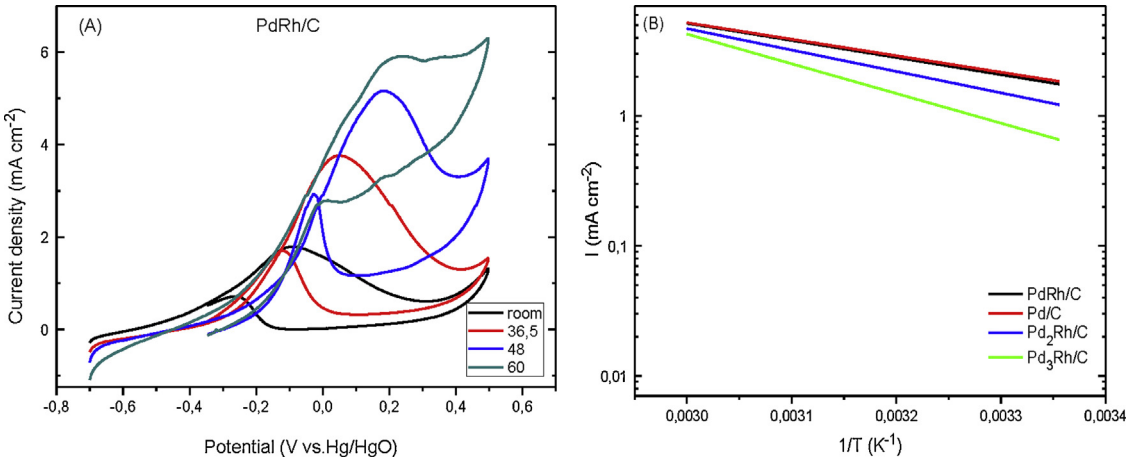

Fig. 7. (A) Cyclic voltammograms of PdRh/C at different temperature values (T = 25, 36.5, 48 and 60 °C), in 0.5 mol L^{-1} KOH containing 0.5 mol L^{-1} glucose, 5 mV s^{-1}, (B) Arrhenius plots for the Pd_xRh/C and Pd/C electrocatalysts derived from cyclic voltammograms at 5 mV s^{-1}.

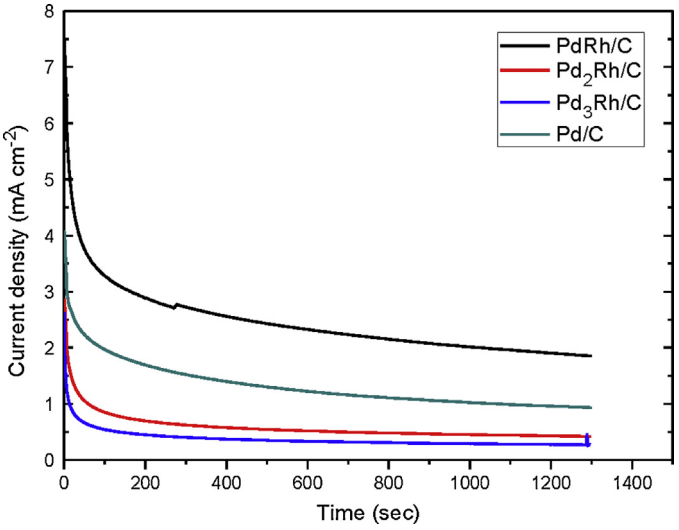

Fig. 8. Chronoamperometric curves at −0.13 V (*vs.* Hg/HgO) for 1300 (s), in a 0.5 mol L^{-1} KOH with 0.5 mol L^{-1} glucose solution.

4. Conclusions

In the present investigation, novel Pd_xRh/C electrocatalysts for glucose electrooxidation were synthesized by a pulse microwave assisted polyol technique and characterized by the XRD, TEM, CV and CA techniques. From TEM characterizations the nanoparticles size was estimated at ~10 nm. Furthermore, according to the electrochemical results the addition of Rh can increase the activity of Pd towards glucose oxidation in alkaline medium. However, PdRh/C is poisoned easier than the other electrocatalysts. The study of the effect of glucose and electrolyte's concentration shows that for 1 mol L^{-1} KOH containing 0.5 mol L^{-1} glucose the highest catalytic activity can be exhibited. For electrolyte's concentration higher than 1 mol L^{-1} KOH the electrocatalytic activity decreases due to the great number of hydroxide ions which may block the glucose's adsorption on the electrode's surface. Finally, it has been found that the increase of temperature until 36.5 °C enhances the electrocatalytic activity, while at higher temperature values the rapid degradation of glucose solution suppresses electrocatalysts' catalytic activity. Consequently, PdRh/C is a good candidate for glucose electrooxidation reaction and further investigation in a direct glucose fuel cell or sensor would be very promising.

Acknowledgements

One of the authors, A. Brouzgou is grateful to European Union (European Social Fund—ESF) and Greek national funds through the Operational Program "Education and Lifelong Learning" of the National Strategic Reference Framework (NSRF)—Research Funding Program: Heracleitus II. Investing in knowledge society through the European Social Fund; that they have co-financed this research. The authors are also grateful to Dr Frusteri Francesco of the CNR-TAE Institute for the TEM analysis.

References

[1] J.P.H. Van Wyk, Trends Biotechnol. 19 (2001) 172–177.
[2] K.C. Swades, R.L. Derek, Nat. Biotechnol. 21 (2003) 1229–1232.
[3] S. Song, W. Zhou, Z. Liang, R. Cai, G. Sun, Q. Xin, V. Stergiopoulos, P. Tsiakaras, Appl. Catal., B 55 (2005) 65–72.
[4] C. Feng, T. Takeuchi, M.A. Abdelkareem, T. Tsujiguchi, N. Nakagawa, J. Power Sources 242 (2013) 57–64.
[5] Y. Wang, S. Song, G. Andreadis, H. Liu, P. Tsiakaras, J. Power Sources 196 (2011) 4980–4986.
[6] G. Andreadis, V. Stergiopoulos, S. Song, P. Tsiakaras, Appl. Catal., B 100 (2010) 157–164.
[7] S. Kerzenmacher, M. Schroeder, R. Brämer, R. Zengerle, F. Von Stetten, J. Power Sources 195 (2010) 6516–6523.
[8] S. Kerzenmacher, U. Kräling, M. Schroeder, R. Brämer, R. Zengerle, F. Von Stetten, J. Power Sources 195 (2010) 6524–6531.
[9] S.C. Barton, H.-H. Kim, G. Binyamin, Y. Zhang, A. Heller, J. Am. Chem. Soc. 123 (2001) 5802–5803.
[10] S.C. Barton, J. Gallaway, P. Atanassov, Chem. Rev. 104 (2004) 4867–4886.
[11] H.-H. Kim, Y. Zhang, A. Heller, Anal. Chem. 76 (2004) 2411–2414.
[12] S. Shleev, J. Tkac, A. Christenson, T. Ruzgas, A.I. Yaropolov, J.W. Whittaker, L. Gorton, Biosens. Bioelectron. 20 (2005) 2517–2554.
[13] R.A. Bullen, T.C. Arnot, J.B. Lakeman, F.C. Walsh, Biosens. Bioelectron. 21 (2006) 2015–2045.
[14] C. Kang, H. Shin, A. Heller, Bioelectrochem. 68 (2006) 22–26.
[15] F. Gao, Y. Yan, L. Su, L. Wang, L. Mao, Electrochem. Commun. 9 (2007) 989–996.
[16] F. Jia, C. Yu, K. Deng, L. Zhang, J. Phys. Chem. C 111 (2007) 8424–8431.
[17] Q. Shen, L. Jiang, H. Zhang, Q. Min, W. Hou, J.-J. Zhu, J. Phys. Chem. C 112 (2008) 16385–16392.
[18] A. Kloke, C. Kloke, R. Zengerle, S. Kerzenmacher, J. Phys. Chem. C 116 (2012) 19689–19698.
[19] C.A. Apblett, D. Ingersoll, S. Sarangapani, M. Kelly, P. Atanassov, J. Electrochem. Soc. (2010) B86–B89.
[20] F. Xie, Z. Huang, C. Chen, Q. Xie, Y. Huang, C. Qin, Y. Liu, Z. Su, S. Yao, Electrochem. Commun. 18 (2012) 108–111.
[21] X. Yan, X. Ge, S. Cui, Nanoscale Res. Lett. 6 (2011) 313.
[22] W. Huang, M. Wang, J. Zheng, Z. Li, J. Phys. Chem. C 113 (2009) 1800–1805.
[23] M. Pasta, R. Ruffo, E. Falletta, C.M. Mari, C.D. Pina, Gold Bull. 43 (2010) 57–64.
[24] D. Basu, S. Basu, Electrochim. Acta 55 (2010) 5775–5779.
[25] D. Basu, S. Basu, Electrochim. Acta 56 (2011) 6106–6113.
[26] D. Basu, S. Basu, Int. J. Hydrogen Energy 36 (2011) 14923–14929.
[27] V. Oncescu, D. Erickson, High volumetric power density, non-enzymatic, glucose fuel cells, Sci. Rep. (2013).
[28] S. Kerzenmacher, U. Kräling, T. Metz, R. Zengerle, F. von Stetten, J. Power Sources 196 (2011) 1264–1272.
[29] N. Fujiwara, S.-i. Yamazaki, Z. Siroma, T. Ioroi, H. Senoh, K. Yasuda, Electrochem. Commun. 11 (2009) 390–392.
[30] S. Ernst, J. Heitbaum, C.H. Hamann, Berichte der Bunsengesellschaft für physikalische Chemie 84 (1980) 50–55.
[31] H. Yin, C. Zhou, C. Xu, P. Liu, X. Xu, Y. Ding, J. Phys. Chem. C 112 (2008) 9673–9678.
[32] J.P. Spets, Y. Kiros, M.A. Kuosa, J. Rantanen, M.J. Lampinen, K. Saari, Electrochim. Acta 55 (2010) 7706–7709.
[33] Z. Liu, L. Huang, L. Zhang, H. Ma, Y. Ding, Electrochim. Acta 54 (2009) 7286–7293.
[34] C. Jin, I. Taniguchi, Mater. Lett. 61 (2007) 2365–2367.
[35] F.M. Cuevas-Muñiz, M. Guerra-Balcázar, F. Castaneda, J. Ledesma-García, L.G. Arriaga, J. Power Sources 196 (2011) 5853–5857.
[36] D. Basu, S. Basu, Int. J. Hydrogen Energy 37 (2012) 4678–4684.
[37] Q. Yi, F. Niu, W. Yu, Thin Solid Films 519 (2011) 3155–3161.
[38] L. An, T.S. Zhao, S.Y. Shen, Q.X. Wu, R. Chen, J. Power Sources 196 (2011) 186–190.
[39] Q. Wang, X. Cui, J. Chen, X. Zheng, C. Liu, T. Xue, H. Wang, Z. Jin, L. Qiao, W. Zheng, RSC Adv. 2 (2012) 6245–6249.
[40] L.-M. Lu, H.-B. Li, F. Qu, X.-B. Zhang, G.-L. Shen, R.-Q. Yu, Biosens. Bioelectron. 26 (2011) 3500–3504.
[41] A. Brouzgou, A. Podias, P. Tsiakaras, J. Appl. Electrochem. 43 (2013) 119–136.
[42] A. Brouzgou, S.Q. Song, P. Tsiakaras, Appl. Catal. B: Environ. 127 (2012) 371–388.
[43] S. Song, Y. Wang, P.K. Shen, J. Power Sources 170 (2007) 46–49.
[44] C. He, S. Song, J. Liu, V. Maragou, P. Tsiakaras, J. Power Sources 195 (2010) 7409–7414.
[45] S. Lee, H.J. Kim, S.M. Choi, M.H. Seo, W.B. Kim, Appl. Catal. A: Gen. 429–430 (2012) 39–47.
[46] X.G. Tang, Q.X. Liu, L.L. Jiang, A.L. Ding, Mater. Chem. Phys. 103 (2007) 329–333.
[47] W. He, H. Jiang, Y. Zhou, S. Yang, X. Xue, Z. Zou, X. Zhang, D.L. Akins, H. Yang, Carbon 50 (2012) 265–274.
[48] A. Pozio, M. De Francesco, A. Cemmi, F. Cardellini, L. Giorgi, J. Power Sources 105 (2002) 13–19.
[49] T. Lopes, E. Antolini, F. Colmati, E.R. Gonzalez, J. Power Sources 164 (2007) 111–114.
[50] R. Pattabiraman, Appl. Catal. A: Gen. 153 (1997) 9–20.
[51] M.H. Seo, S.M. Choi, H.J. Kim, W.B. Kim, Electrochem. Commun. 13 (2011) 182–185.
[52] Z.X. Liang, T.S. Zhao, J.B. Xu, L.D. Zhu, Electrochim. Acta 54 (2009) 2203–2208.
[53] T. Takamura, i.K. Minamiyama, J. Electrochem. Soc. 112 (1965) 333–335.
[54] J. Prabhuram, R. Manoharan, H.N. Vasan, J. Appl. Electrochem. 28 (1998) 935–941.
[55] M. Grdeń, A. Czerwiński, J. Solid State Electrochem. 12 (2008) 375–385.
[56] M.C. Jeong, C.H. Pyun, I.H. Yeo, J. Electrochem. Soc. 140 (1993) 1986–1989.
[57] L. Vračar, S. Burojević, N. Krstajić, Int. J. Hydrogen Energy 23 (1998) 1157–1164.
[58] I. Becerik, F. Kadirgan, Electrochim. Acta 37 (1992) 2651–2657.
[59] L. Meng, J. Jin, G. Yang, T. Lu, H. Zhang, C. Cai, Anal. Chem. 81 (2009) 7271–7280.
[60] B.K. Boggs, G.G. Botte, Electrochim. Acta 55 (2010) 5287–5293.
[61] T. Maiyalagan, K. Scott, J. Power Sources 195 (2010) 5246–5251.
[62] M.A. Abdel Rahim, R.M. Abdel Hameed, M.W. Khalil, J. Power Sources 134 (2004) 160–169.

[63] M. Noroozifar, M. Khorasani-Motlagh, R. Khaleghian-Moghadam, M.-S. Ekrami-Kakhki, M. Shahraki, J. Solid State Chem. 201 (2013) 41–47.
[64] C.-C. Hu, T.-C. Wen, Electrochim. Acta 39 (1994) 2763–2771.
[65] E. Laviron, J. Electroanal. Chem. Interfacial Electrochem. 101 (1979) 19–28.
[66] E. Laviron, L. Roullier, J. Electroanal. Chem. Interfacial Electrochem. 115 (1980) 65–74.
[67] H. Tang, J. Chen, S. Yao, L. Nie, Y. Kuang, Z. Huang, D. Wang, Z. Ren, Mater. Chem. Phys. 92 (2005) 548–553.
[68] J. Wang, Anal. Electrochem. Can. (2006).
[69] M. Shamsipur, M. Najafi, M.-R.M. Hosseini, Bioelectrochem 77 (2010) 120–124.
[70] I. Becerik, Turk. J. Chem. 23 (1999) 57–66.
[71] L.H.E. Yei, B. Beden, C. Lamy, J. Electroanal. Chem. 246 (1988) 349–362.
[72] S.T. Nguyen, D.S. Ling Tan, J.-M. Lee, S.H. Chan, J.Y. Wang, X. Wang, Int. J. Hydrogen Energy 36 (2011) 9645–9652.
[73] Y. Wang, T.S. Nguyen, X. Liu, X. Wang, J. Power Sources 195 (2010) 2619–2622.
[74] Z.H. Teng, G. Wang, B. Wu, Y. Gao, J. Power Sources 164 (2007) 105–110.